HYDROTHERMAL SYNTHESIS OF TITANIA POWDERS AND THEIR PHOTOCATALYTIC PROPERTIES

VÁCLAV ŠTENGL, SNEJANA BAKARDJIEVA, NATALIYA MURAFA, VENDULA HOUŠKOVÁ

Institute of Inorganic Chemistry, AS CR, v.v.i., Řež 250 68, Czech Republic

E-mail: houskova@iic.cas.cz

Submitted April 14, 2008; accepted September 18, 2008

Keywords: Anatase, Rutile, Hydrothermal synthesis, Photocatalytic activity

Nanocrystalline titanium (IV) dioxide powders with particle size in the range 30 to 45 nm and surface area in the range from 150 to 600 m^2/g were prepared by hydrothermal treatment of aqueous $TiO_2.xH_2O$ suspension which was synthesized from aqueous solutions of $TiOSO_4$, $TiOCl_2$, TiCl4 and $TiCl_3$, respectively, by chemical reaction with 1M ammonium hydroxide. The structure of prepared samples was determined by X-ray powder diffraction (XRD) and selected area electron diffraction (SAED). The morphology and microstucture characteristics were also obtained by scanning electron microscopy (SEM) and high resolution electron microscopy (HRTEM). The nitrogen adsorption-desorption was used for determination of surface area (BET) and porosity. The photocatalytic activity of the prepared titania samples were assessed by photocatalytic decomposition of Orange II dye in an aqueous slurry under UV irradiation at 365 nm wavelength. The best photocatalytic activity showed the samples of gel precursors prepared from $TiCl_4$ and $TiCl_3$. The result suggests that the photocatalytic activity on the decomposition of Orange II dye depends on the particle size of samples prepared by hydrothermal synthesis.

INTRODUCTION

Titanium dioxide, also known as titania is the naturally occurring oxide of titanium. We will find TiO_2 in all kinds of paint, printing ink, plastics, paper, synthetic fibers, rubber, condensers, painting colours and crayons, ceramics, electronic components along with food and cosmetics. Many studies have been published on the use of TiO_2 as a photocatalyst for the decomposition of organic compounds. Photocatalytic activity (PCA) is the ability of a material to create an electron hole pair as a result of exposure to ultraviolet radiation. The resulting free-radicals are very efficient oxidizers of organic matter. Photocatalytic activity in TiO_2 has been extensively studied because its potential use in sterilization, sanitation, and remediation applications. The ability to control PCA is important in many other applications utilizing TiO_2 including paint pigments and cosmetics that require low PCA. The photocatalytic activity of titania results in thin coatings of the material exhibiting self cleaning and disinfecting properties under exposure to UV radiation. These properties make the material a candidate for applications such as medical devices, food preparation surfaces, air conditioning filters, and sanitaryware surfaces.

Nanocrystalline anatase [1] powders with particle sizes from 8 to 38 nm have been synthesized by hydrothermal treatment of aqueous $TiOSO_4$ solutions and $TiO_2.xH_2O$ amorphous gel. In the next work [2], anatase-type TiO_2, which was stable up to 800°C, was successfully synthesized from $TiOSO_4$ under hydrothermal condition at 180°C and its photocatalytic activity through the decomposition of methylene blue in aqueous solution as a function of calcination conditions was studied. Photocatalytic activity of anatase [3] powders was discussed in the relation to their crystallinity. Anatase powders were synthesized under hydrothermal condition at 180°C from $TiOSO_4$ aqueous solution with 0.1-3.0 mol/l concentration and then annealed at high temperatures above 700°C. Titania samples rich in brookite [4] were prepared under hydrothermal conditions by starting from $TiCl_3$ as titanium precursor. Nanocrystalline titania with particle size 20-50 nm and specific surface area 20-80 m^2/g was prepared by hydrothermal treatment of aqueous solution $TiOSO_4$, $H_2TiO(C_2O_4)_2$ and $TiO(NO_3)_2$ solutions[ ]. The photocatalytic behavior of synthesized TiO2 powders was studied in the reaction of phenol photodegradation in water and optimal characteristics of these materials are explored. The best photocatalytic activity was observed for a mixture of rutile (15 %) and anatase (85 %) prepared by high-temperature hydrolysis of aqueous $TiOSO_4$ solution. Nanocrystalline zirconia and titania [6] were synthesized by hydrothermal treatment of zirconyl $ZrO(NO_3)_2$ and titanyl $TiO(NO_3)_2$ nitrates aqueous solutions and amorphous gels of the corresponding hydroxides, the hydrothermal synthesis was performed in the range of temperatures 150-250°C. Nanocrys-

talline powders of anatase and rutile type of titania with different morphology and particle size 13-50 nm (XRD) were prepared by a hydrothermal treatment of complex titanyl oxalate acid $H_2TiO(C_2O_4)_2$ aqueous solutions [7]. A titanium hydroxide nanogel was neutrally precipitated from a $TiCl_4$ aqueous solution and then used as the precursor in the hydrothermal process [8]. The application of microwave irradiation to the hydrothermal synthesis of rutile from aqueous $TiOCl_2$ solution is presented in paper [9]. Mesoporous nanocrystalline TiO_2 powders were synthesized by a hydrothermal method using tetrabutylorthotitanate as precursor in ethanol-water mixed solutions [10]. Nanosized TiO_2 particles were prepared by hydrothermal method of the amorphous powders which were precipitated in an aqueous peroxotitanate solution using different amine group-containing organics [11]. Well-defined spherical mesoporous TiO_2 was prepared from a poly(ethylene glycol)-poly(propylene glycol)-based triblock copolymer and titanium isopropoxide mixed with 2,4-pentanedione by using a simple sol-gel approach in aqueous solution. Hydrothermal treatment was performed to increase the crystallinity, thermal stability, surface area, and photocatalytic activity of the mesoporous TiO_2 [12]. TiO_2 nanoparticles were prepared using the hydrolysis of titanium tetraisopropoxide using tetraethyl ammonium hydroxide as a peptizing agent in the hydrothermal method [13]. Industrial $TiOSO_4$ solution was used as inorganic precursor to prepare mesoporous titania via composite template route, using cetyltrimethylammonium bromide (CTAB) and tri-block copolymer EO20PO70EO20 (P-123) as structure-directing agents (SDA) under high acidity conditions [14]. Trimodally sponge-like macro-mesoporous titania was prepared by hydrothermal treatment of precipitates of tetrabutyl titanate ($Ti(OC_4H_9)_4$) in pure water [15]. Bimodal nanocrystalline mesoporous TiO_2 powders with high photocatalytic activity were prepared by a hydrothermal method using tetrabutylorthotitanate $TiO(C_4H_9)_4$ as precursor [16]. Highly photoactive nano-sized TiO_2 powder photocatalyst was prepared by a hydrothermal method at 180°C for 5 h using tetrabutyl titanite (TBOT) as the precursor. The pH values of the starting suspensions were adjusted from 1 to 11 using a 1.0 M HCl or 1.0 M $NH_3{\cdot}H_2O$ solution [17]. TiO_2 powder (Degussa P25) was hydrothermally treated in pure water at 150°C for different times. The results showed that a small amount of anatase was transformed into rutile phase and more aggregates of the TiO_2 crystallites formed after hydrothermal treatment, resulting in the decrease of specific surface area of the TiO_2 powders [18].

In this work the formation process of titania during hydrothermal synthesis starting from an amorphous $TiO_2.xH_2O$ gel has been investigated. The UV photocatalytic activities of the as-prepared samples were tested by the degradation of 0.02M Orange 2 dye solutions. Under the same conditions, the photocatalytic activity of the commercially available photocatalyst (Degussa P25) was examined.

EXPERIMENTAL

Preparation of titania precursors

All used chemicals, $TiOSO_4$, $TiOCl_2$, $TiCl_4$, NH_4OH and metal titanium were supplied by Fluka Munich Germany. Amorphous titania precursor (P1-P4) was prepared by five different routes. The titanium salts were precipitated at temperature 0°C in cooling bath with ice. The white amorphous precipitates were washed with distilled water and decanted.

Precursor P1: By-product of titania amorphous gel from production of titania white by Precheza Přerov Ltd., Czech Republic. End samples are denoted as AUT_4, AUT_10 and AUT_12.

Precursor P2: 15 g of $TiOSO_4$ was diluted in 500 ml of distilled water and precipitated with 1M solution of ammonium hydroxide. End sample is denoted as AUT_13.

Precursor P3: 15 ml of $TiOCl_2$ hydrochloric acid solution (Ti 15 %, HCl 38-42 %) was dissolved in 250 ml of distilled water and precipitated with 1 M solution of ammonium hydroxide. End sample is denoted as AUT_14.

Table 1. Experimental conditions, BET, pore size distribution and rate constant of prepared samples.

Sample	Precursor	Reaction Time (days)	XRD Analysis	Ccrystallite size (nm)	Surface area (m^2/g)	Average pore radius (nm)	Total pore volume (cm^3/g)	Rate constant k (min^{-1})
Aut_4	P1	3	Anatase	38.1	178.0	1.535	0.09	0.0208
Aut_10	P1	5	Anatase	34.5	149.7	1.529	0.06	0.0185
Aut_12	P1	7	Anatase	31.6	182.1	1.529	0.07	0.0154
Aut_13	P2	3	Anatase	19.1	450.4	1.528	0.17	0.0049
Aut_14	P3	3	Anatase	11.2	599.5	6.230	0.28	0.0158
Aut_15	P4	3	Anatase	23.8	273.3	1.528	0.08	0.0245
Aut_26	P5	3	Rutile	69.3	54.5	6.190	0.16	0.0236
P25	-	-	A/R	20.8/33.1	50.5	1.54	0.09	0.0416

Precursor P4: 10 ml of $TiCl_4$ solution (0,1M in 20% HCl) was dissolved in 250 ml of distilled ice water and precipitated with 1 M solution of ammonium hydroxide. End sample is denoted as AUT_15.

Precursor P5: 2 g of metal Ti was dissolved in 5 ml conc. HCl and diluted with 250 ml of distilled water. The purple solution of $TiCl_3$ was precipitated with 1M ammonium hydroxide solution. End sample is denoted as AUT_26.

Hydrothermal synthesis of titania powders

The amorphous gel precursor $TiO_2.xH_2O$ (see Table 1) obtained by reaction with ammonium hydroxide was transferred into 100 ml quartz cartouche held in stainless steel autoclave. After flush with flow of nitrogen, the autoclave was slowly heated from room temperature to the temperature of 250°C at the rate of 5°C/min by the PID controller. Then the reaction was maintained at this temperature for 3-7 days. The autoclave was removed from the oven and free cooled to room temperature. The product was removed from the quartz cartouche, washing with decantation, filtered off and dried at the oven at the temperature of 105°C.

Characterization methods

Specific surface areas of the samples were determined by nitrogen adsorption-desorption isotherms at liquid nitrogen temperature using a Quantachrome Nova 2000 instrument with NovaWin2 version 2.1. software. In each case, prior to measurement the samples were degassed in a flowing nitrogen atmosphere at 150°C for 5 h in a separate degassing unit. Specific surface area was calculated by the BET method [19], while the pore size distribution (pore diameter and pore volume) was determined by the BJH method [20].

Transmission electron microscopy was carried out by two instruments: Philips EM 201 at 80 kV and JEOL JEM 3010 at 300 kV (LaB_6 cathode). Copper grid coated with a holey carbon support film was used to prepare samples for TEM observation. Powder was dispersed in ethanol and the suspension was treated in ultrasonic bath for 10 minutes.

SEM studies were performed using a Philips XL30 CP microscope equipped with EDX, Robinson, SE and BSE detectors. The sample was placed on an adhesive C slice and coated with 10-nm-thick Au-Pd alloy layer.

X-ray powder diffraction patterns were obtained on a Siemens D5005 instrument using Cu Kα radiation (40 kV, 30 mA) and diffracted beam monochromator. Crystallite size of the samples was calculated from the Scherrer [21] equation using the X-ray diffraction peak at $2\Theta = 25.3°$ (anatase) and $2\Theta = 27.4°$ (rutile). Qualitative analysis was performed with the Eva Application and the Xpert HighScore using the JCPDS PDF-2 database [22].

Photocatalytic activity of samples was assessed from the kinetics of the photocatalytic degradation of 0.02 M Orange II dye (OII) in aqueous slurries. Kinetics of the photocatalytic degradation of aqueous Orange II dye solution was measured by using the photoreactor [23]. This photoreactor consists of a stainless steel cover and quartz tube with florescent lamp (365 nm, 8 W). Orange II dye solution circulated by means of membrane pump through the flow cuvette. The concentration of Orange II dye was determined by measuring absorbance at 480 nm with VIS spectrofotometer ColorQuestXE. The concentrations calculated the peak areas were plotted as a function of the irradiation time. The software OriginPro 7.5 was used to fit normalized kinetic curve of first-order kinetics to the experimental points. For comparison, an analogous experiment with the standard photocatalyst TiO_2–P25 (Degussa) was carried out.

RESULTS AND DISCUSSION

X-Ray Diffraction (XRD)

XRD of the amorphous titania starting materials (precursors P2-P4) showed that there are no peaks present. XRD of the precursor P1 (Figure 1a) showed anatase diffraction peaks with low intensity. The XRD patterns of the titanium oxide prepared by hydrothermal reaction of titania precursors (Figure 1b-g) comport with a single phase of anatase (ICDD PDF 21-1272). Figure 1h presented the pure rutile phase prepared from $TiCl_3$ solution (ICDD PDF 21-1276). No other polymorph of titania was observed. The broadening of diffraction peaks indicates small size of nanocrystals. The average size t of crystallites was calculated from the peak half-width B using the Sherrer equation [17]:

$$t = \frac{k\lambda}{B\cos\Theta} \tag{1}$$

where k is a shape factor of the particle (it is 1 if the spherical shape is assumed), λ and Θ are the wavelength and the incident angle of the X-rays, respectively. The peak width was measured at half of the maximum intensity. The crystallite size calculated from diffraction plane (101) of anatase and diffraction plane (110) of rutile is summarized in Table 1. The crystallite size decreased with the reaction time of hydrothermal synthesis and depends on the origin of amorphous gel.

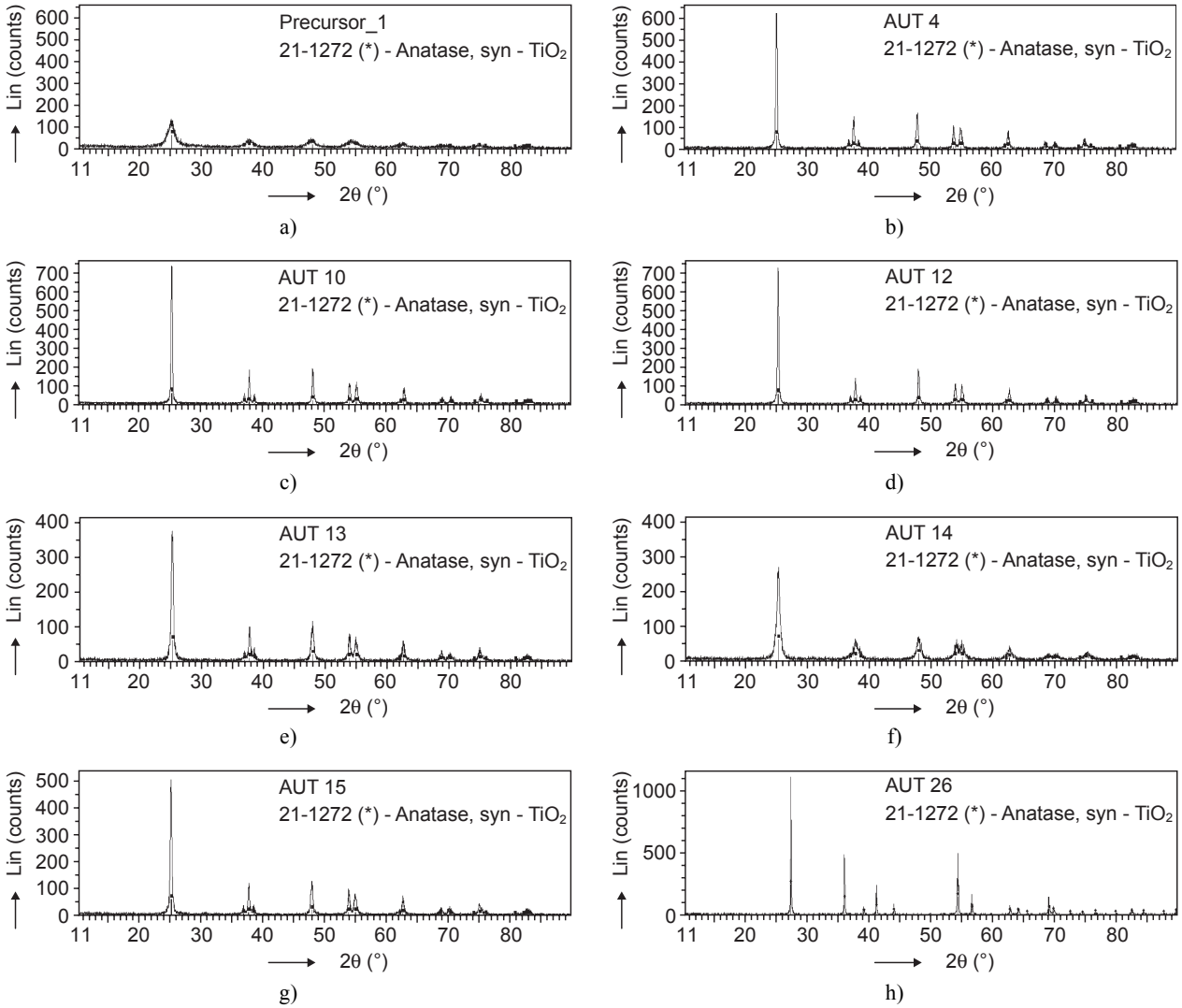

Figure 1. XRD pattern of presursor P1 (a) and samples AUT_4 (b), AUT_10 (c), AUT_12 (d), AUT_13 (e), AUT_14 (f), AUT_15 (g), AUT_26 (h).

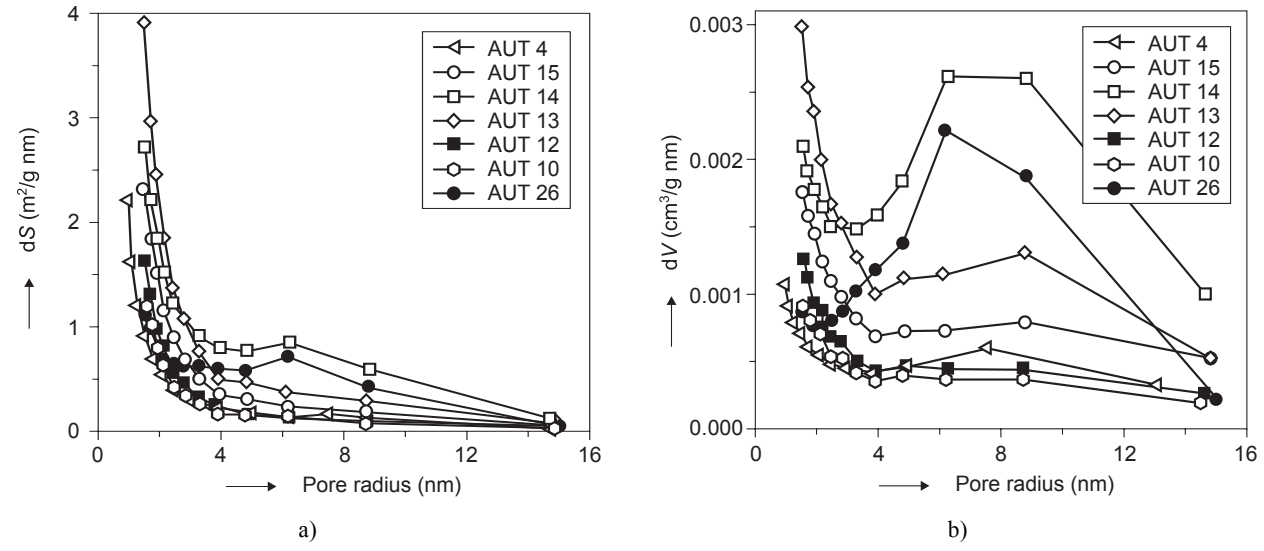

Figure 2. Desorption BJH pore area distribution (a) and pore volume distribution (b).

Surface area and porosity of prepared samples

All prepared samples give an isotherm of type II with an A hysteresis loop according to the IUPAC classification [24]. This kind of isotherm is indication of nonporous powders or powders with pore diameters larger than micropores. Type A hysteresis is due principally to cylindrical pores open at both ends. Pore area distribution and pore volume distribution calculated by BJH method are presented in Figure 2a and Figure 2b. The pores with diameters around 8 nm are dominant for all prepared samples. Specific surface area is presented in Table 1. The highest value of surface area had sample prepared from $TiOCl_2$ (~ 600 m^2/g), the lowest value of surface area (150 m^2/g) had sample prepared after five days hydrothermal reaction of Precheza Ltd. by-product.

Electron microscopy SEM, HRTEM and ED

The morphology of synthesized titania powder observed by SEM is shown in Figure 3. In this picture, there are presented, as an example, samples denoted as AUT_4 and AUT_10. The morphology of the others prepared samples is analogous. The SEM and HRTEM (Figure 4 a,b) micrographs show roughly spherical particles of 40 nm size. At higher magnification in the TEM micrographs, small subunits forming the agglomerates can be observed. HRTEM image shows small anatase microcrystals forming the clumps.

High-resolution transmission electron microscopy techniques were used to characterize the fine structure of titanium dioxide prepared by hydrothermal synthesis. Image processing analysis of HRTEM micrograph was used to achieve in refinement of microstructure in the sense that we can more accurately analyse grains and grains boundaries. Furthermore, it is possible to determine and index crystallographic planes from Fourier transform and find their orientations. The area used for image processing is region of the original image taken with mask 512×512 pixels. Microstructure of the prepared samples is determined utilizing Fast Fourier Transformation analysis techniques (FFT) for quantify the lattice spacing.

The HRTEM micrographs in Figures 4a-d characterize the surface morphology of the sample obtained after three days of hydrothermal synthesis and denoted as AUT_4. Figure 5a-d represent sample obtained after five days of hydrothermal synthesis (AUT_10). The crystalline areas are firm in all the parts of platelet crystal. The fine fringe spacing is 0.35 nm (Figure 4c,d and Figure 5c,d) and corresponding to the (011) plane of anatase, the fine fringe spacing of 0.24 nm corresponds to the (013) plane of anatase (see Figure 4c).

HRTEM images of titania crystallites (Figure 6) obtained by hydrothermal synthesis of gels prepared from $TiOSO_4$ (sample denoted as AUT_13) shows type of domain corresponding to TiO_2 space-group I41/amd. The unit cell of anatase has been used to index the ED pattern (calculated by FFT) inserted in Figure 6c. The motive in Figure 6c corresponds to (110) plane. The fine fringe spacing of 0.35 nm (Figure 6d) corresponds to the (011) anatase plane.

HRTEM images of titania crystallites prepared by hydrothermal synthesis of gels prepared from $TiOCl_2$ and $TiCl_4$, respectively, are presented in Figures 7 and 8 (samples denoted as AUT_14 and AUT_15). The fine fringe spacing of 0.35 nm (Figure 7c and 8d) corresponds to the (011) anatase plane and the fine fringe spacing calculated by FFT method (Figure 7d and 8c) corresponds to (101) plane of anatase unit cell.

Sample denoted as AUT_26 was prepared by hydrothermal synthesis of gel precursor prepared from $TiCl_3$. The crystalline areas are firm in all the parts of narrow crystal. The fine fringe spacing is 0.32 nm (Figure 9d) and corresponds to the (110) rutile plane.

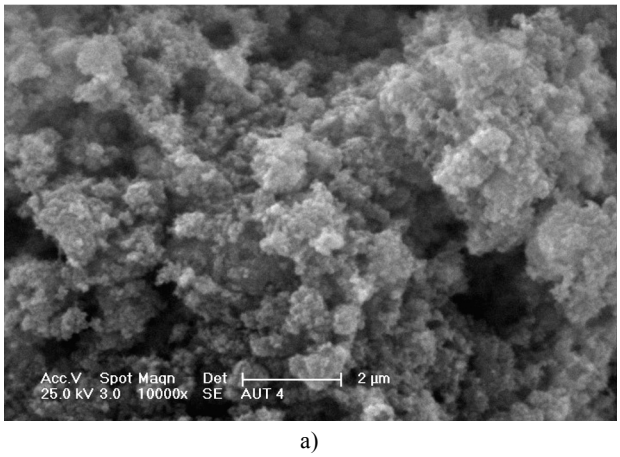

a)

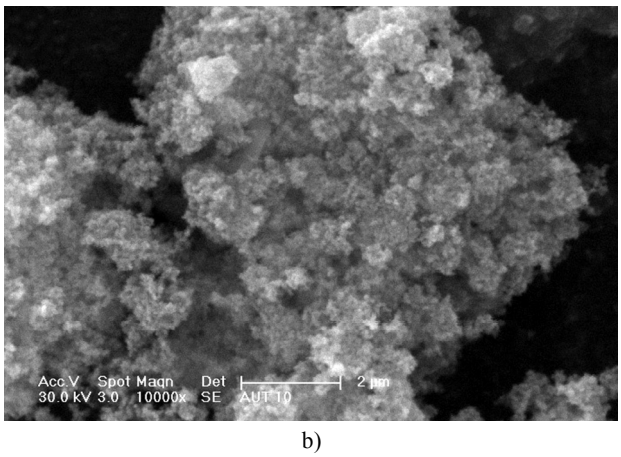

b)

Figure 3. SEM images of sample AUT_4 (a) and sample AUT_10 (b).

Diffraction methods are the most important sources of microstructure information to identify individual microscopic-sized crystallites, i.e. to identify the crystallographic phase the crystallite corresponds to. Structure determination is generally based on selected area electron diffraction (SAED) patterns in the transmission electron microscope (TEM). A computer program ProcessDiffraction [25] helps indexing a set of single crystal selected area electron diffraction (SAED) patterns by determining which of the presumed structures can fit all the measured patterns simultaneously. Distances and angles are measured in the digitalized patterns with a graphical tool by clicking on the two shortest non-collinear vectors (spots), using user-supplied calibration data. Next figures depicts the selected electron diffraction patterns (SAED) analyzed by ProcessDiffraction program. In these images are for example presented SAED of sample denoted as AUT_10 (anatase) and AUT_26 (rutile). Figure 10a represents the structure of anatase (ICDD PDF 21-1272) and Figure 10b shows the structure of rutile (ICDD PDF 21-1272).

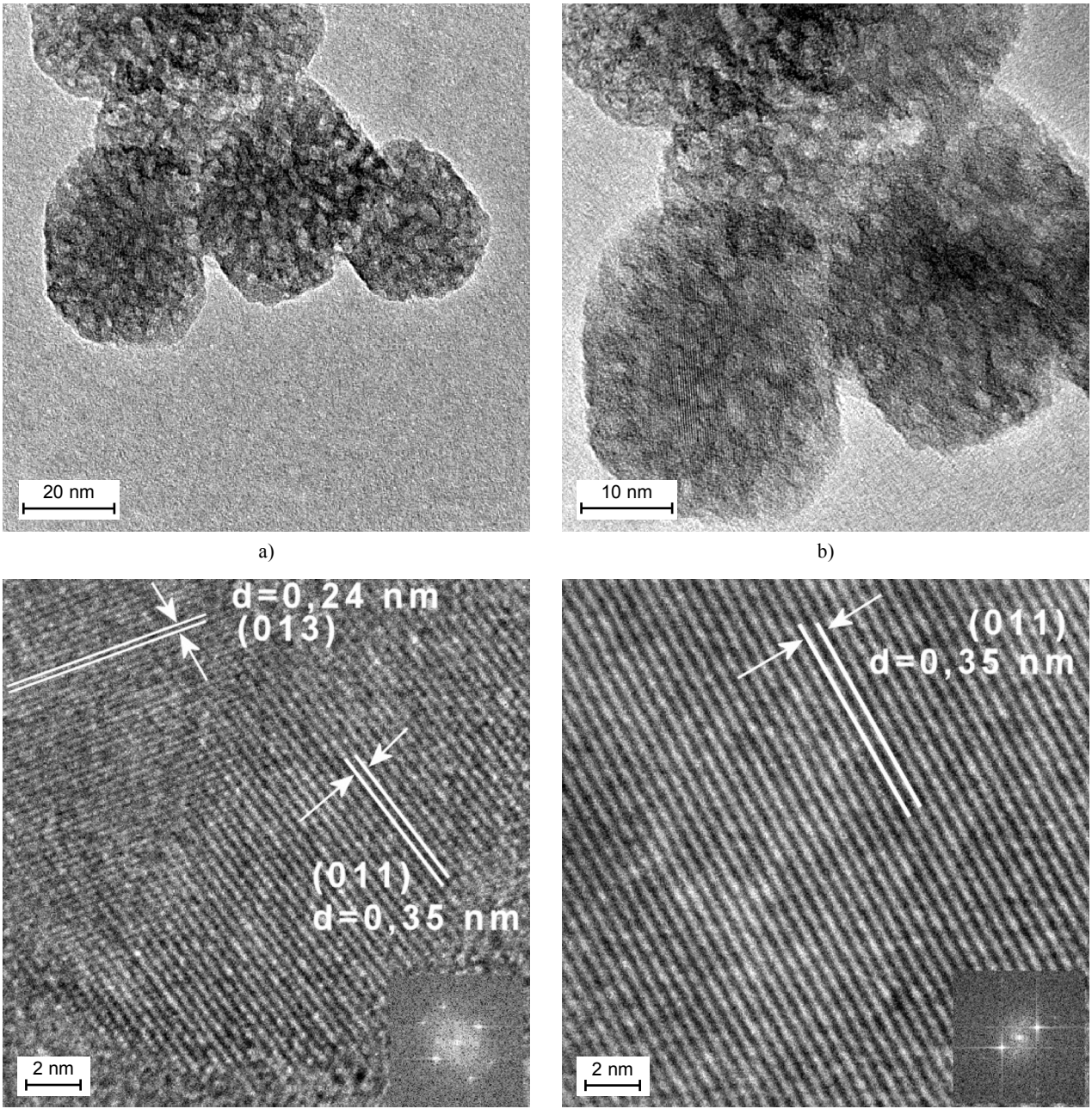

Figure 4. HRTEM micrographs of sample AUT_4 (a). Images (b), (c) and (d) are enlarged parts of the image (a).

Photocatalytic activity

The photocatalytic activity of the prepared samples was determined by degradation of 0.02 M Orange II dye aqueous solutions under UV radiation at 365 nm wavelength. In regions where the Lambert-Beer law is valid, the concentration of the Orange II dye is proportional to absorbance.

$$A = \varepsilon\, c\, l \tag{2}$$

where A is absorbance, c is concentration of absorbing component, l is length of absorbing layer and ε is molar absorbing coefficient. The time dependences of Orange 2 dye decomposition can be described by using Equation (3) for the first-order kinetics reaction:

$$\frac{d[OII]}{dt} = k \cdot [OII] \tag{3}$$

where [OII] is concentration of Orange II dye and k is rate constant. It is visible from Figure 11 that the first order kinetics curves (plotted as lines) fitted to all experimental points. For comparison, the photocatalytic activity of a commercially available photocatalyst

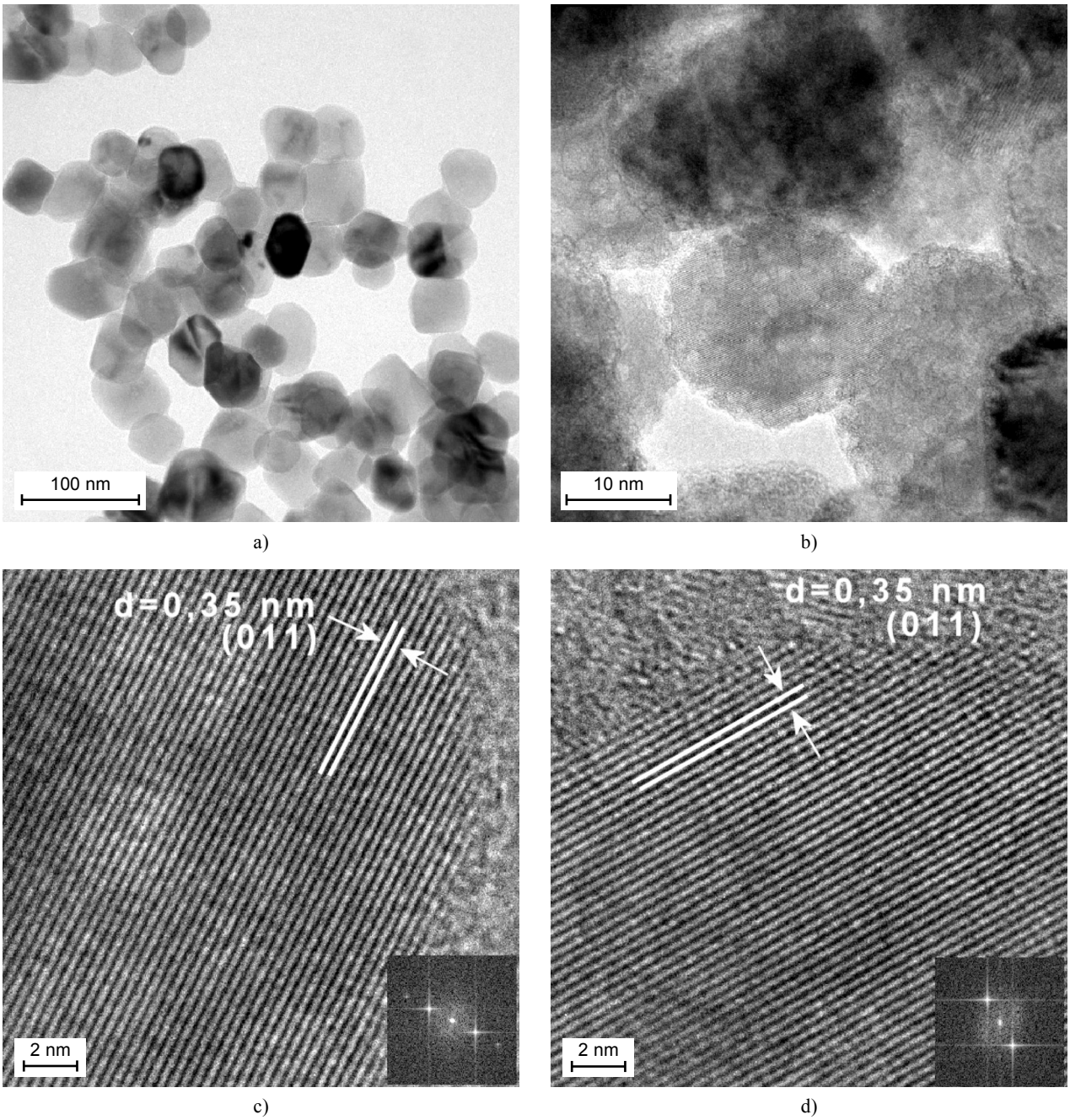

Figure 5. HRTEM micrographs of sample AUT_10 (a). Images (b), (c) and (d) are enlarged parts of the image (a).

(Degussa P25) was also tested. The calculated degradation rate constants are listed in Table 1 and degradation kinetics of Orange II dye at 365 nm wavelength of the all prepared samples are presented in Figure 11.

From results in Table 1 follow that titania powders prepared by hydrothermal synthesis exhibits lower photocatalytic activity for degradation of aqueous Orange II dye than reference sample P25 (Degussa). For pure TiO_2, the e^- and h^+ recombination may be grouped into two categories: volume recombination and surface recombination. Volume recombination is a dominant process in well-crystallized large TiO_2 particles [26], which can be reduced by decreasing particle size. Reduction in particle size also leads to larger surface area, which increases the available surface active sites. Surface recombination becomes an important process when particle size becomes extremely small, about 1-10 nm [23].

From the results it is evident that the kind of precursor has effect on the end product. The samples prepared from commercial product and from precursor prepared from $TiOSO_4$ have larger particle size (20-30 nm)

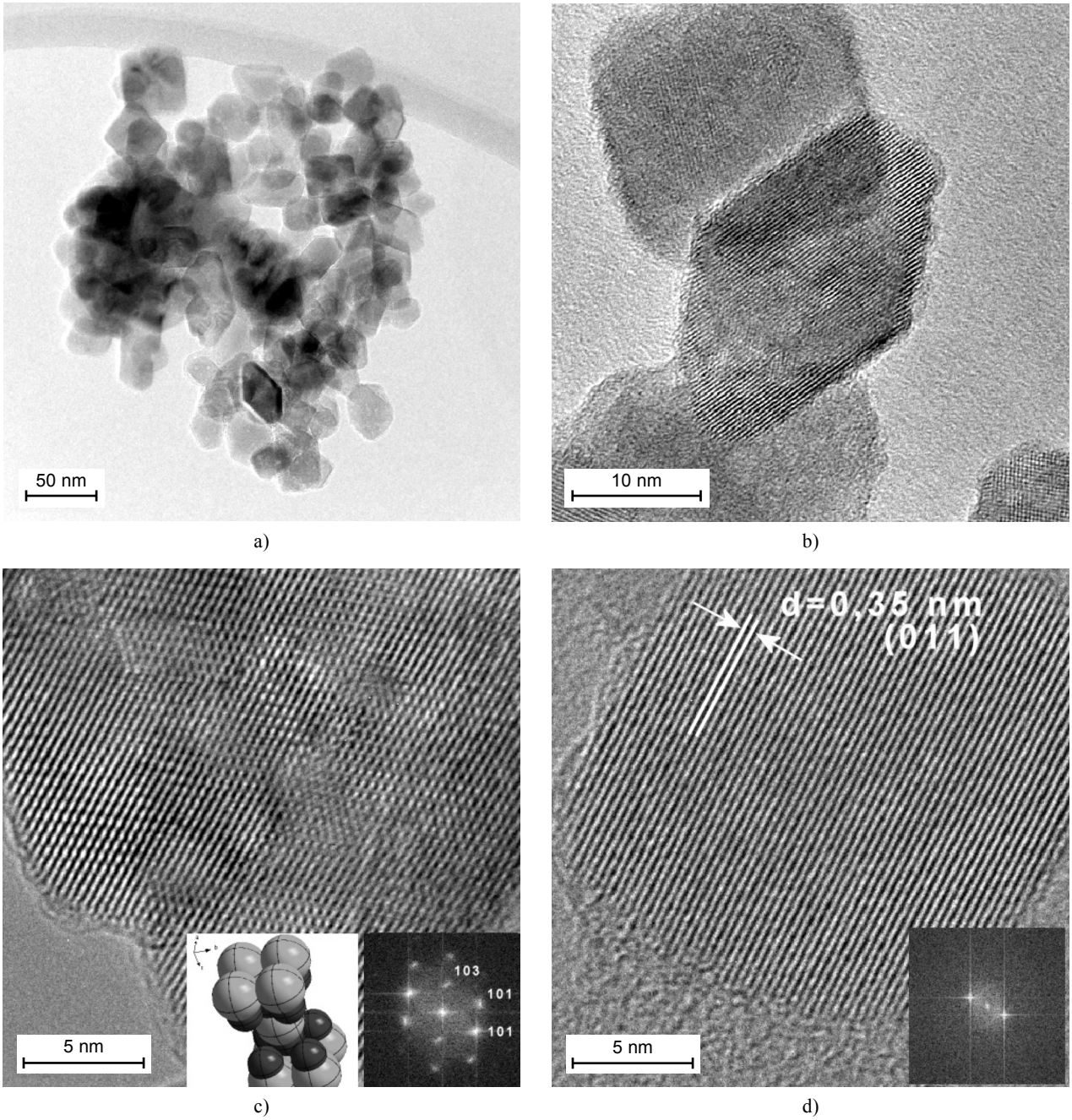

Figure 6. HRTEM micrographs of sample AUT_13 (a). Images (b), (c) and (d) are enlarged parts of the image (a).

and lower surface area. In Figure 4a-b is displayed nucleus from by-product of amorphous gel which recrystallize into anatase during the hydrothermal process. This sample was compared with AUT_13 - with well-developed crystal structure and poor photocatalytic activity. Samples prepared from Precursor P1 achieved decreasing activity with increasing reaction time (3-7 days) in the autoclave (see Tab. 1). These times have influence on crystallite size and surface area and pore volume too. It can be said that activities of samples prepared from precursor P1 increase with increasing crystallite size. Sample AUT_13 prepared from precursor P2 had very poor activity which was caused probably by low crystallite size and poor crystallinity (see Figure 13b). Sample AUT_14 and AUT_15 prepared from precursor P3 and P4 represent direct proportion between the crystallite size and the photocatalytic activity and inverse proportion between the surface area and the photocatalytic activity. These results imply that photocatalytic activity increase with crystallite size to the size limit and over this limit is decreased. The products prepared from chloride precursors

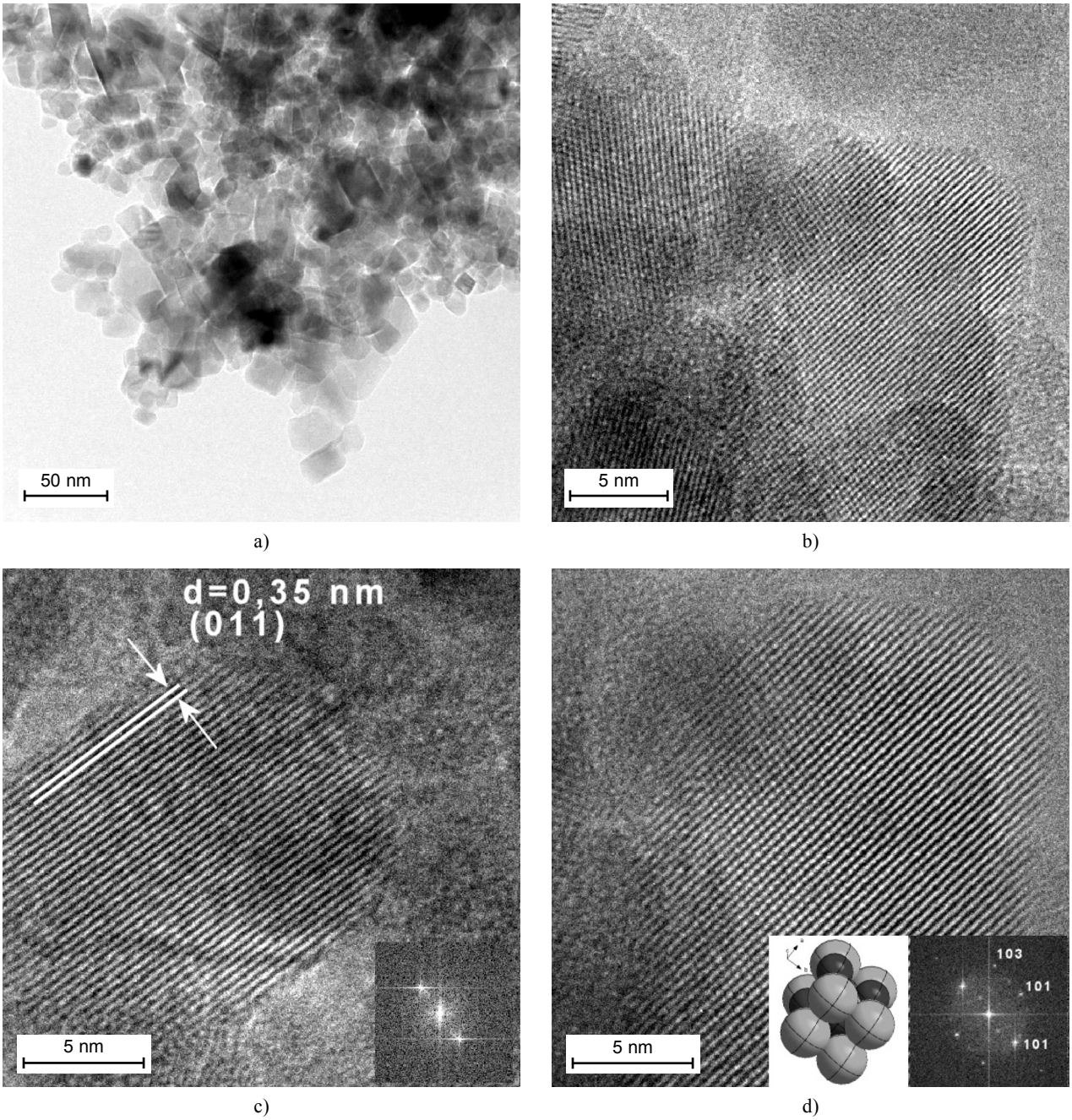

Figure 7. HRTEM micrographs of sample AUT_14 (a). Images (b), (c) and (d) are enlarged parts of the image (a).

(AUT_14 and AUT_15) have the highest photocatalytic activity thanks to the high surface area. Fall in photocatalytic activity of the sample AUT_14 prepared from $TiOCl_2$ is obviously caused by the fall in crystal size to 10 nm. Unanticipated high photocatalytic activity had sample prepared from $TiCl_3$ precursor (AUT_26). In comparison with other samples, it has the largest particle size and the lowest surface area. Sample AUT_26 was prepared from $TiCl_3$, therefore oxygen vacancies and trivalent titanium (Ti^{3+}) may be present in the modified TiO_2. The oxygen vacancies and Ti^{3+} species act as hole traps [27]. Once the oxygen vacancies and Ti^{3+} species combined with the holes they turn into charged species. At the same time, oxygen acts as electron trap during the reaction. Thereafter, the trapped holes transfer to the organic substrate leading to a degradation reaction and the charged defects recover original states of oxygen vacancies and Ti^{3+}. Both the oxygen vacancies and Ti^{3+} were attributed to the enhancement of photocatalytic activity of the sample denoted as AUT_26. High photocatalytic activity is associated with small crystallite sizes because small crystallite size

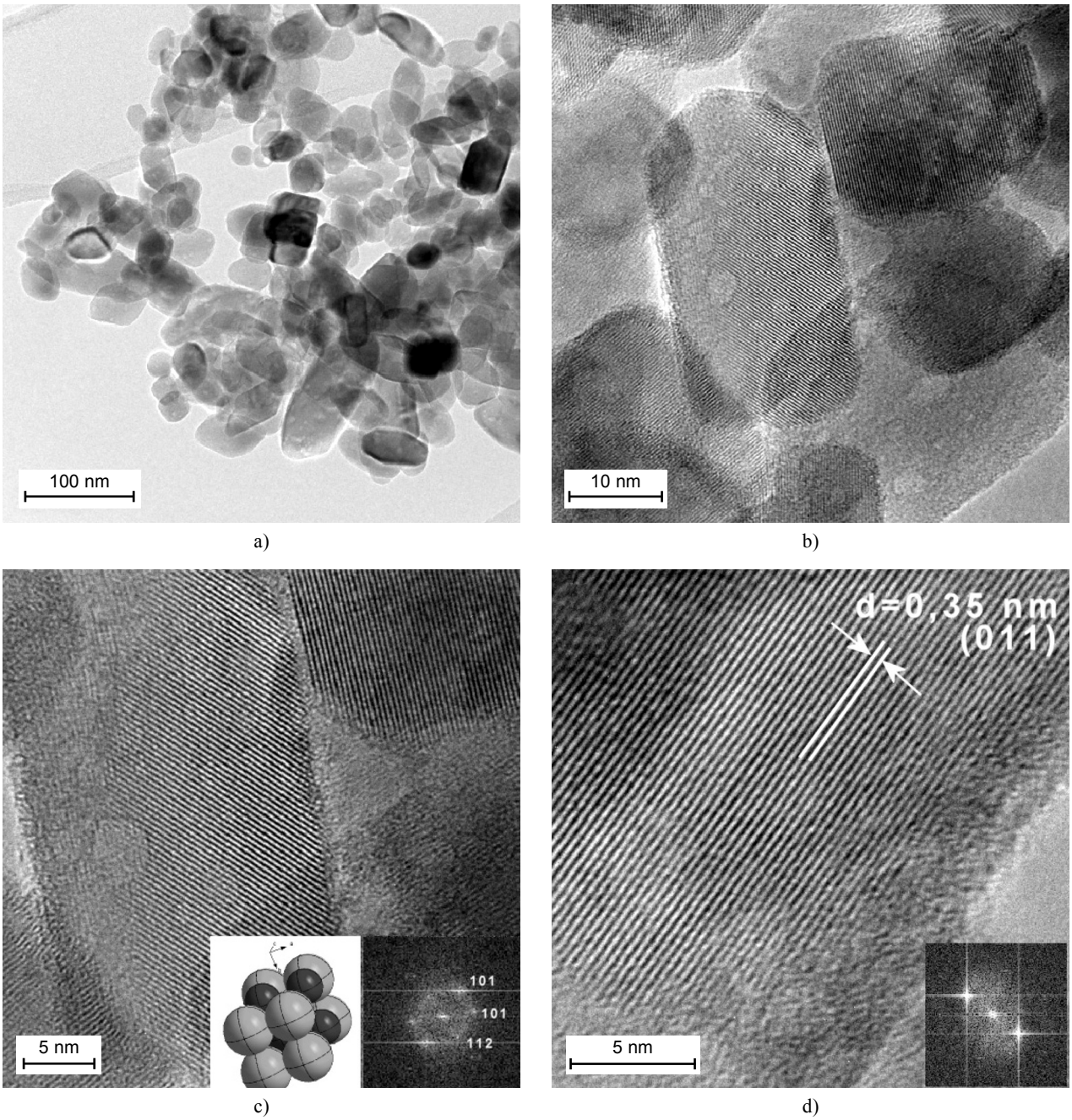

Figure 8. HRTEM micrographs of sample AUT_15 (a). Images (b), (c) and (d) are enlarged parts of the image (a).

can lead to quantum size effects in semiconductors [28]. This result suggests that the photocatalytic activity on the decomposition of Orange II depends on the particle size. It means the activity increases with a decreasing particle size. It is consistent with the result that the photocatalytic reaction has a small particle-size effect, wherein the photocatalytic activity increases with a decrease of particle size [ ]. Titanium dioxide can take on any of the following three crystal structures: anatase, rutile and brookite. Anatase type titanium dioxide photocatalyst generally exhibits higher photocatalytic activity than the other types of titanium dioxide as regards the decomposition of organic pollutants by suppressing the electron-hole recombination. In the case of AUT_26 sample, the rutile phase prepared from $TiCl_3$ shows higher photocatalytic activity than anatase by reason of oxygen vacancies and trivalent titanium.

CONCLUSION

In the present work, we successfully synthesized nanocrystalline titania powders by a hydrothermal method and investigated their photocatalytic properties

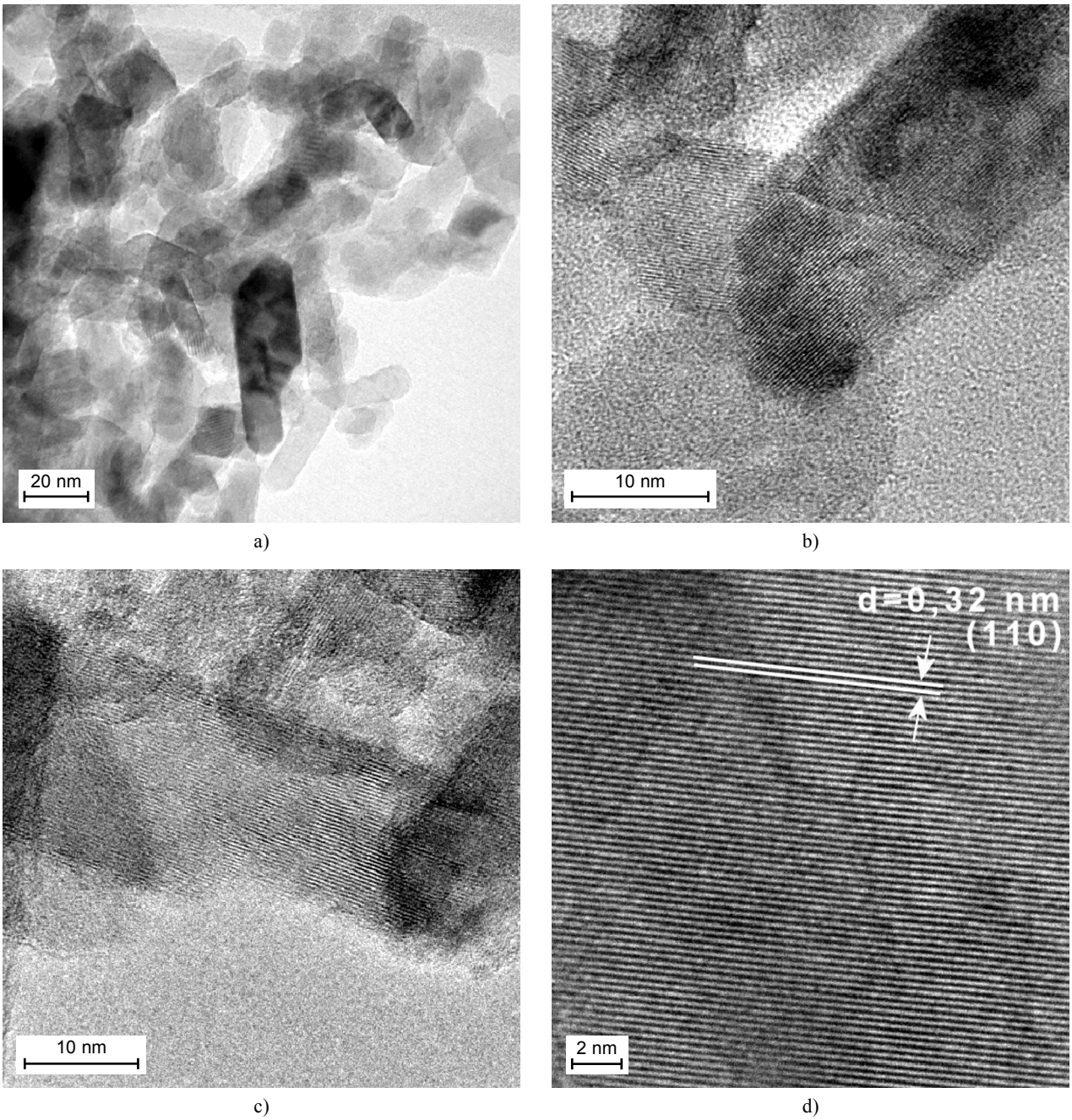

Figure 9. HRTEM micrographs of sample AUT_26 (a). Images (b), (c) and (d) are enlarged parts of the image (a).

in details. The best photocatalytic activity showed the samples of gel precursors prepared from $TiCl_4$ and $TiCl_3$, respectively. The result suggests that the photocatalytic activity on the decomposition of Orange II dye depends on the particle size. The photocatalytic activity of titania powders was found to decrease with increasing reaction time of hydrothermal synthesis. Also effect of hydrothermal synthesis in autoclave caused that rutile has had higher photoactivity than anatase even though in the majority of cases anatase achieve higher activity.

Acknowledgement

The work was supported by the Academy of Sciences of the Czech Republic (Project No. AV0Z40320502) and by the Grant Agency of the Czech Republic GAČR (project No. 203/08/0334).

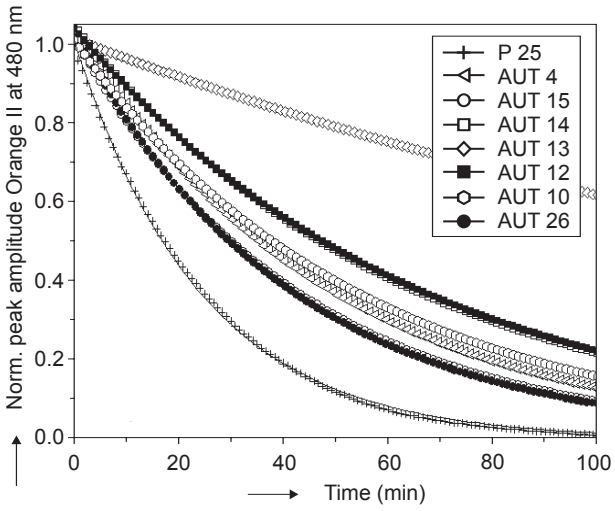

Figure 11. Photocatalytic activity of prepared titania powders and photocatalyst Deggusa P25 at 365 nm wavelength.

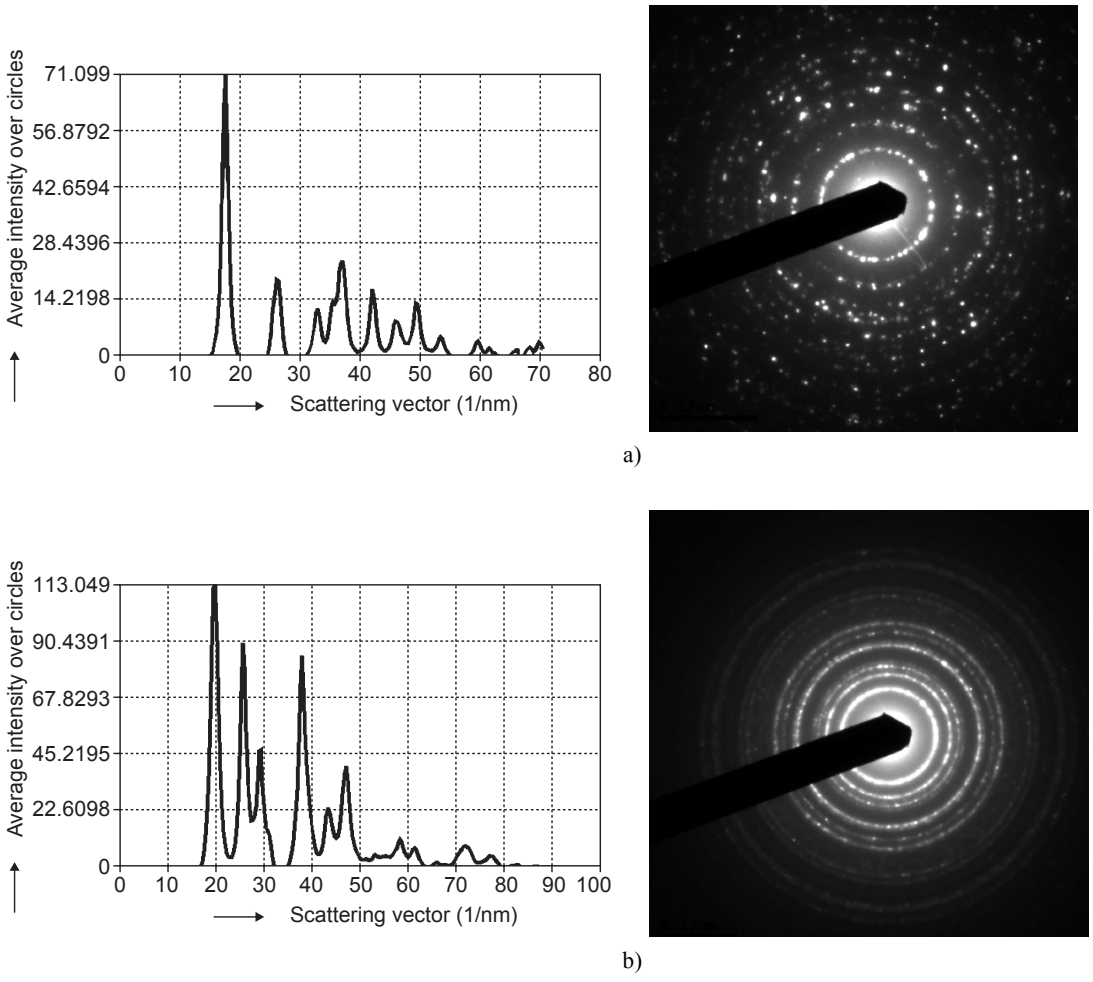

Figure 10. Electron diffraction pattern of anatase - sample AUT_10 (a) and rutile (b)- sample AUT_26.

References

1. Kolen'ko Y. V., Burukhin A. A., Churagulov B. R., Oleynikov N. N.: Materials Letters *57*, 1124 (2003).
2. Inagaki M., Nakazawa Y., Hirano M., Kobayashi Y., Toyoda M.: J. Inorg. Mater. *3*, 809 (2001).
3. Toyoda M., Nanbu Y., Nakazawa Y., Hirano M., Inagaki M.: Appl. Catal. B: Environ. *49*, 227 (2004).
4. Bokhimi X., Pedraza F.: J. Solid State Chem. *177*, 2456 (2004).
5. Kolen'ko Y. V., Churagulov B. R., Kunst M., Mazerolles L., Colbeau-Justin C.: Appl. Catal. B: Environ. *54*, 51 (2004).
6. Kolen'ko Y. V., Maximov V. D., Burukhin A. A., Muhanov V. A., Churagulov B. R.: Mat. Sci. Eng. C *23*, 1033 (2003).
7. Kolen'ko Y. V., Maximov V. D., Garshev A. V., Meskin P. E., Oleynikov N. N., Churagulov B. R.: Chem. Phys. Lett. *388*, 411 (2004).
8. Cho C. H., Han M. H., Kim D. H., Kim D. K.: Mat. Chem. Phys. *92*, 104 (2005).
9. Baldassari S., Komarneni S., Mariani E., Villa C.: Mat. Res. Bull. *40*, 2014 (2005).
10. Wang G.: J. Mol. Catal. A: Chem. *274*, 185 (2007).
11. Ryu Y. B., Sig M. L., Jeong E. D., Kim H. G., Jung W. Y., Baek S. H., Lee G. D., Park S. S., Hong S. S.: Catal. Today *124*, 88 (2007).
12. Kim D. S., Klak S. Y.: Appl. Catal. A: Gen. *323*, 110 (2007).
13. Kim J. H., Jung W. Y., Baek S. H., Lim K. T., Lee G. D., Park S. S., Hong S. S.: Chem. Eng. Sci. *62*, 5154 (2007).
14. Tian C., Zhang Z., Hou J., Luo N.: Mat. Lett. *62*, 77 (2008).
15. Yu J., Zhang L., Cheng B., Su Y.: J. Phys. Chem. C *111*, 10582 (2007).
16. Yu J., Wang G., Cheng B., Zhou M.: Appl. Catal. B: Env. *69*, 171 (2007).
17. Yu J., Su Y., Cheng B., Zhou M.: J. Mol. Catal. A: Chem. *258*, 104 (2006).
18. Yu J., Yu H., Cheng B., Zhou M., Zhao X.: J. Mol. Catal. A: Chem. *253*, 112 (2006).
19. Brunauer S., Emmett P. H., Teller E.: J. Am. Chem. Soc. *60*, 309 (1938).
20. Barret E. P., Joyner L. G., Halenda P. P.: J. Am. Chem. Soc. *73* (1951), 373-380.
21. Scherrer P.: Gott. Nachr. *2*, 98 (1918).
22. JCPDS PDF-2 release 2001, ICDD Newtown Square, PA, USA.
23. Monteagudo J. M., Duran A.: Chemosphere *65*, 1242 (2006).
24. Lowell S., Shields J. E.: *Powder Surface Area and Porosity*, Chapman&Hall, London, 1998.
25. Labár J. L.: Ultramicroscopy *103*, 237 (2005).
26. Sermone N. D., Lawless D., Khairutdinov R.: J. Phys. Chem. *99*, 16655 (1995).
27. Liu H., Wu H. J., Sun F. X., Yao Y. L., Wu M., Li W. Z.: J. Mol. Catal. *15*, 47 (2001).
28. Wang Y., Herron N.: J. Phys. Chem. *95*, 525 (1991).
29. Fujishima A., Hashimoto K., Watanabe T.: *TiO_2 Photocatalysis: Fundamentals and Application*, p. 124, BKC, Tokyo 1999.

HYDROTERMÁLNÍ PŘÍPRAVA TiO_2 PRÁŠKŮ A JEJICH FOTOKATALYTICKÉ VLASTNOSTI

VÁCLAV ŠTENGL, SNEJANA BAKARDJIEVA, NATALIYA MURAFA, VENDULA HOUŠKOVÁ

Ústav anorganické chemie, AV ČR, v.v.i., Řež 250 68

Hydrotermálními postupy z prekurzoru $TiO_2.xH_2O$ byl připraven nanokrystalický oxid titaničitý mající velikost částic 30 až 45 nm a měrný povrch 150 až 600 m^2g^{-1}. Prekurzor byl získán reakcí vodných roztoků $TiOSO_4$, $TiOCl_2$, $TiCl_4$ respektive $TiCl_3$ s 1M roztokem hydroxidu amonného. Struktura připravených vzorků byla charakterizována pomocí rentgenové difrakce (XRD) a elektronové difrakce (SAED). Morfologie a mikrostruktura vzorků byla analyzována pomocí skenovací elektronové mikroskopie (SEM) a vysokorozlišovací transmisní elektronové mikroskopie (HRTEM). K určení měrného povrchu (BET) a porozity prášků byla použita metoda adsorpce (desorpce) dusíku. Fotokatalytická aktivita připravených prášků byla určena pomocí rozkladu barviva Oranž II ve vodném prostředí a to UV zářením o vlnové délce 365 nm. Nejlepší fotokatalytické vlastnosti vykazovaly vzorky připravené reakcí s $TiCl_4$ a $TiCl_3$. Z výsledků vyplývá, že rychlost rozkladu barviva a tím i fokatalytická aktivita závisí na velikosti částic prášků připravených hydrotermální syntézou.